Chemical Science

ROYAL SOCIETY OF CHEMISTRY

EDGE ARTICLE

View Article Online
View Journal | View Issue

Cite this: *Chem. Sci.*, 2024, **15**, 13201

All publication charges for this article have been paid for by the Royal Society of Chemistry

Biomimetic engineering of a neuroinflammation-targeted MOF nanozyme scaffolded with photo-trigger released CO for the treatment of Alzheimer's disease†

Chun Liu,[ab] Wenting Zhang,[ab] Haochen Zhang,[ab] Chuanqi Zhao,[ab] Xiubo Du,[c] Jinsong Ren[ab] and Xiaogang Qu[*ab]

Alzheimer's disease (AD) is one of the most fatal and irreversible neurodegenerative diseases, which causes a huge emotional and financial burden on families and society. Despite the progress made with recent clinical use of inhibitors of acetylcholinesterase and amyloid-β (Aβ) antibodies, the curative effects of AD treatment remain unsatisfactory, which is probably due to the complexity of pathogenesis and the multiplicity of therapeutic targets. Thus, modulating complex pathological networks could be an alternative approach to treat AD. Here, a neutrophil membrane-coated MOF nanozyme (denoted as Neu-MOF/Fla) is biomimetically engineered to disturb the malignant Aβ deposition–inflammation cycle and ameliorate the pathological network for effective AD treatment. Neu-MOF/Fla could recognize the pathological inflammatory signals of AD, and deliver the photo-triggered anti-inflammatory CO and MOF based hydrolytic nanozymes to the lesion area of the brain in a spontaneous manner. Based on the *in vitro* and *in vivo* studies, Neu-MOF/Fla significantly suppresses neuroinflammation, mitigates the Aβ burden, beneficially modulates the pro-inflammatory microglial phenotypes and improves the cognitive defects of AD mice models. Our work presents a good example for developing biomimetic multifunctional nanotherapeutics against AD by means of amelioration of multiple symptoms and improvement of cognitive defects.

Received 19th April 2024
Accepted 17th July 2024

DOI: 10.1039/d4sc02598a

rsc.li/chemical-science

Introduction

Alzheimer's disease (AD) is one of the most fatal neurodegenerative diseases, which affects millions of people throughout the world and causes a huge family and social burden.[1–3] Emerging evidence indicates that the deposition of amyloid-β (Aβ) in the brain is the key hallmark in the progress of AD.[4,5] Current treatments targeting the Aβ, such as small molecules,[6–8] metal complexes,[9] peptides or antibodies,[10,11] and nanomaterials[12,13] have been constructed to eliminate Aβ and block Aβ aggregation. Although there have been some benefits, most have failed in the clinical trials and remain unsatisfactory.[14,15] This is probably because pathological progression in AD is orchestrated by multiple factors, and improvement of one or a few may not be adequate to prevent or reverse disease progression.[16–18] Many indicators of inflammation are found in AD: elevated levels of immune molecules, over activated microglia (the brain-resident immune cells), and increased changes in the specialized vasculature of the blood–brain barrier (BBB) support the hypothesis that inflammation is an integral part of AD.[19,20] Plentiful clinical trials for Alzheimer's drugs have hit a roadblock because of a series of inflammation events caused by these drugs.[21,22] Moreover, highly insoluble Aβ deposition in the illness is regarded as classical stimulants of inflammation, causing excessive production of inflammatory factors and abnormal activation of glial cells, thus exacerbating neuroinflammation.[23–25] In turn, in neuroinflammation, the γ-secretase modulatory protein, IFITM3, is expressed in neurons and astrocytes induced by inflammatory cytokines, and is responsible for upregulating the activity of γ-secretase, thereby increasing the production of Aβ;[26] on the other hand, dysfunctional microglia and astrocytes decrease the phagocytosis and clearance of Aβ, thus further promoting Aβ deposition.[27] This malignant Aβ deposition–inflammation cycle severely exacerbates disease progression and greatly increases the difficulty of treatment of AD. Therefore, it is of interest to develop alternative strategies that conquer the complexity and diversity of the pathological network for effective AD treatment.[17]

[a]*Laboratory of Chemical Biology and State Key Laboratory of Rare Earth Resource Utilization, Changchun Institute of Applied Chemistry, Chinese Academy of Sciences, Changchun, Jilin 130022, P. R. China. E-mail: xqu@ciac.ac.cn*

[b]*University of Science and Technology of China, Hefei, Anhui, 230026, P. R. China*

[c]*College of Life Sciences and Oceanography, Shenzhen Key Laboratory of Microbial Genetic Engineering, Shenzhen University, Shenzhen 518060, China*

† Electronic supplementary information (ESI) available. See DOI: https://doi.org/10.1039/d4sc02598a

Currently, studies have demonstrated that carbon monoxide (CO) serves as an intrinsic gas neurotransmitter and exhibits anti-inflammatory effects, thus endowing it with potential drug activity.[28–30] It is believed that CO plays a key role in the alleviation of oxidative stress and the inhibition of inflammation for neuroprotection in AD.[31–33] As such, the efficient delivery of CO in the brain for neuroinflammation management is a promising alternative strategy to treat AD. Several CO releasing molecules (CORMs) have been used to deliver CO; however, there are still key issues to overcome for biomedical applications. These CORMs have aroused a series of problems in the inflammation treatment because of their nonspecific biodistribution, fast renal excretion, poor tissue permeability, and low retention at pathological sites.[34] In view of the advancement of nanotransport systems, an ideal CO nanocarrier with targeted delivery, high loading capacity, optimized physicochemical properties and biocompatibility is highly desired but challenging.[35–40]

In the past few decades, nanozymes have received much attention;[41–43] this is not only due to their specific enzyme-like activities but also retaining their intrinsic multifunctional repertoires, such as magnetic heat[44] and photocatalytic properties.[37] Recently, metal–organic framework (MOF)-based nanozymes have been widely used owing to their microporosity, uniformly structured cavity, catalytically active sites and adjustable surface functionality.[45–47] However, more than 90% of existing studies focus on redox enzyme mimics, while only a small fraction focused on hydrolytic enzyme mimics.[48] A Zr(IV)-based MOF, MOF-808, has been verified to be an excellent heterogeneous catalyst for catalytic peptide bond hydrolysis in a large number of peptides.[49] Meanwhile, the excellent pore structure of MOF-808 is expected to be ideal for efficient CORM loading. With this in mind, we attempt to construct a MOF based hydrolytic nanozyme with CO delivery, which is expected to disrupt the malignant Aβ deposition–inflammation cycle and ameliorate the pathological network for effective AD treatment.

Here, we have developed neutrophil membrane-coated MOF nanozymes (named Neu-MOF/Fla) and employed them in neuroinflammation management as well as clearance of Aβ plaques for AD treatment. Cell membrane coating strategies have been widely applied to deliver drugs to homotypic cancer cells,[50] or inflammatory sites.[51] It has been demonstrated that neutrophils can be attracted by pro-inflammatory factors and chemoattractants, spontaneously crossing the BBB and homing in on neurons during the process of neuroinflammation in AD.[52–54] In this context, a neutrophil cell membrane is utilized for inflammation targeting and BBB penetration. As illustrated in Scheme 1, the MOF-808 nanoparticles are used for encapsulating Fla, a photo-induced CORM (MOF/Fla).[55,56] Then MOF/Fla is further coated with a neutrophil cell membrane to obtain Neu-MOF/Fla. In an Alzheimer's mouse model, the administrated Neu-MOF/Fla could cross the BBB and migrate to the inflammatory sites. Subsequently, Neu-MOF/Fla achieves *in situ* rapid photo-induced CO release and degradation of Aβ. The smart designed neutrophil membrane-based MOF hydrolytic nanozyme with CO delivery is explored for the first time, showing great potential as a candidate for AD treatment.

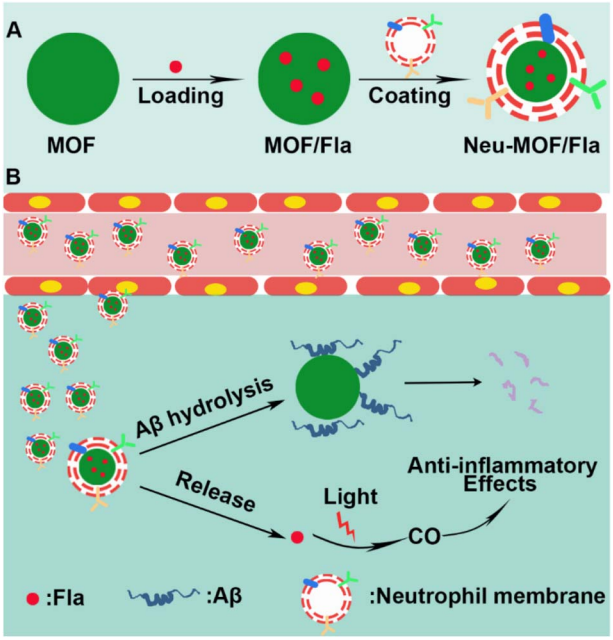

Scheme 1 Schematic illustration of (A) Neu-MOF/Fla synthesis and (B) neutrophil membrane-targeted *in situ* CO release and degradation of Aβ for synergistic treatment of AD.

Results and discussion

As illustrated in Scheme 1A, Neu-MOF/Fla was constructed in three steps. First, MOF-808 nanoparticles were synthesized by the microwave irradiation method according to previous literature.[57] The transmission electron microscopy (TEM) as well as scanning electron microscopy (SEM) images suggested the MOFs had a uniform octahedral morphology with a diameter of about 80 nm (Fig. 1A and S1). The X-ray diffraction (XRD) patterns revealed that the diffraction peaks could be well indexed to the reported crystalline MOF-808 (Fig. S2†).[57] Second, Fla was encapsulated into MOF-808 for CO release. Before encapsulating Fla, the nitrogen adsorption–desorption experiment was carried out to evaluate the porous properties. As shown in Fig. 1B, a clear hysteresis at higher p/p_0 was observed, indicating the creation of mesoporous in MOF-808. In addition, the BET surface area and average pore size of MOF-808 were determined to be 913.49 $m^2\ g^{-1}$ and 3.01 nm, respectively. The high porosity and large surface area made it promising for efficient drug loading. Afterwards, the Fla synthesized as previously reported[58] was loaded into the porous MOF-808 under ultrasonication and stirring (MOF/Fla). The fluorescence and absorption spectra of the MOF/Fla suspension showed an obvious characteristic peak of Fla, indicating that Fla was successfully loaded into MOF-808 (Fig. S3 and S4†). Most visibly, the MOF-808 nanoparticles changed from white to pale yellow in color after Fla loading (Fig. S5†). Moreover, the Fourier transform infrared (FTIR) spectrum and the XRD patterns of MOF/Fla were closely analogous to that of pure MOF-808, indicating that the incorporation of Fla had negligible interference on the structure of MOF-808 carriers (Fig. S6 and S7†).

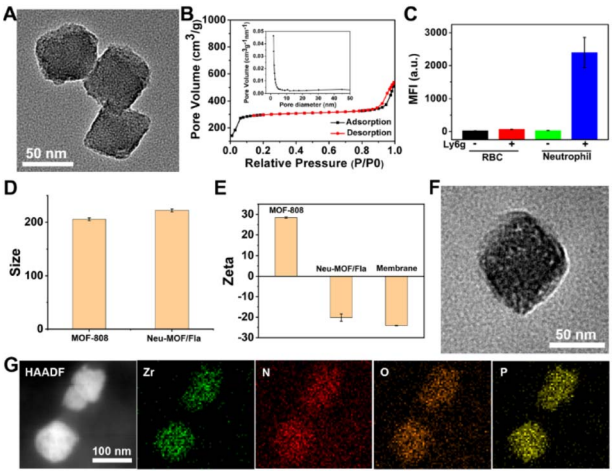

Fig. 1 (A) TEM images of MOF-808. The ethanol solution of the samples was dripped onto formvar stabilized with carbon support films for the test. (B) Nitrogen adsorption–desorption curves of MOF-808. Inset figure: pore size distributions derived from the adsorption branch. (C) Flow cytometric analysis of the purity of neutrophils stained with FITC-conjugated Ly6g antibodies. (D) DLS measurements of MOF-808 and Neu-MOF/Fla. (E) Zeta potential of MOF-808, Neu-MOF/Fla and the neutrophil membrane. The samples were dispersed in an aqueous solution. (F) TEM images of Neu-MOF/Fla. (G) HAADF-STEM image and elemental mapping for neutrophil membrane-coated MOF-808.

The loading capacity reached a satisfactory value of 15%, as determined by using UV-vis spectra. Third, MOF/Fla was further coated with a neutrophil cell membrane derived from purified and activated mouse bone marrow neutrophils (Fig. 1C, S8 and S9) to obtain Neu-MOF/Fla. Explanatorily, red blood cells (RBCs) were chosen as a control because they had analogous structures to neutrophils, but RBCs are less plastic in traversing the BBB and migrating to an inflamed brain compared to neutrophils.[51,52] The average hydrodynamic size of Neu-MOF/Fla increased to ~17 nm after membrane coating by dynamic light scattering (DLS) measurements (Fig. 1D). Meanwhile, the surface zeta potential of Neu-MOF/Fla was dramatically reduced from 28.4 mV to −20.2 mV, matching the surface zeta potential of the neutrophil membrane vesicles (Fig. 1E). In addition, the TEM image showed that Neu-MOF/Fla had an obvious neutrophil membrane coating (Fig. 1F). The elemental mapping further suggested the successful coating of a neutrophil membrane (Fig. 1G). Sodium dodecyl sulfate-polyacrylamide gel electrophoresis (SDS-PAGE) additionally supported the preservation of membrane proteins in Neu-MOF/Fla (Fig. S10†). Overall, all the quality assurance specifications for the preparation of Neu-MOF/Fla were employed to ensure physicochemical and biological reproducibility of the nanoparticles.

In AD, Aβ are known to activate microglia and produce chemoattractants for reliable recruitment of neutrophils, during which they transmigrate in the central nervous system and play an important role in neuroinflammation.[53,59] We next examined whether Neu-MOF/Fla could target the activated inflammatory cells. Before cell-based studies, we first evaluated the biocompatibility of Neu-MOF/Fla. There was no obvious reduction in the cell viability under our experimental conditions, indicating the low cytotoxicity and acceptable biocompatibility of Neu-MOF/Fla (Fig. S11†). Then, we selected BV2 cells, a cell in the brain responsible for immune and inflammatory regulation, and tested if they could be activated by $A\beta_{40}$. A significant rise in expression levels of CD16 (a pro-inflammatory phenotype marker) of BV2 cells was observed after treatment with $A\beta_{40}$ (Fig. S12†). Then, Neu-MOF/Fla was added to BV2 cells activated with $A\beta_{40}$, while RBC-MOF/Fla was tested as a control. Fla has been demonstrated to be useful for fluorescence imaging *in vitro* and *in vivo*.[56,60] After incubation with Neu-MOF/Fla, the cells showed an obvious fluorescence, but no significant fluorescence was observed for the cells incubated with RBC-MOF/Fla (Fig. 2A). Furthermore, flow cytometry analysis also showed a significant enhancement in fluorescence after incubation with Neu-MOF/Fla (Fig. 2B). These results indicated that Neu-MOF/Fla was able to target inflamed BV2 cells with the assistance of the neutrophil membrane coating. This is mainly due to the protein–receptor interactions mediated by CD11b on the neutrophil membrane.[61,62]

Then, we examined the CO-releasing capability of Neu-MOF/Fla, which plays prominent roles in neuroinflammation

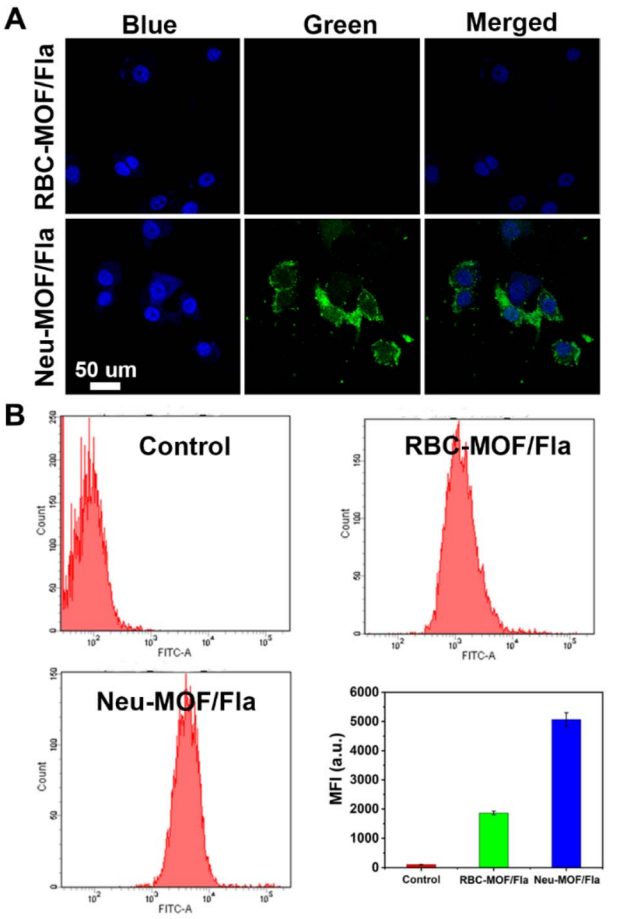

Fig. 2 (A) Fluorescence images and (B) flow cytometric analysis of BV2 cells after incubation with RBC-MOF/Fla (25 μg mL^{-1}) and Neu-MOF/Fla (25 μg mL^{-1}), respectively. Cells were activated with $A\beta_{40}$ before being treated with nanoparticles.

management. The schematic CO-releasing reaction of Fla is shown in Fig. 3A. It has been reported that the CO release of Fla causes the loss of emission features, and it is is easy to achieve "real-time" monitoring of CO release from fluorescence changes. In the presence of irradiation, gradual reduction of the fluorescence of Neu-MOF/Fla was observed within 6 min (Fig. 3B). Moreover, the color of Neu-MOF/Fla solution changed from pale yellow to colorless after irradiation (Fig. S13†). Since the reactive product had no fluorescent signal, this indicated that the release of CO was efficient during irradiation. Meanwhile, as shown in Fig. 3C, irradiation resulted in ~60% conversion to CO within 6 min. Subsequently, we investigated the intracellular CO release of Neu-MOF/Fla in BV2 cells using confocal microscopy. After incubation with Neu-MOF/Fla, the BV2 cells showed good uptake, as indicated by the evident emission in the green channel (Fig. 3D). When the cells were irradiated for 10 min, an apparent disappearance of the emission was observed in the green channel, but not in the blue channel (Fig. 3D). Furthermore, a fluorescent CO probe was used to detect the intracellular release of CO. As shown in Fig. S14,† the fluorescence intensity of the cells treated with Neu-MOF/Fla was remarkably enhanced under illumination, while that of the control in the absence of Neu-MOF/Fla or illumination exhibited rather weak fluorescence. The above results demonstrated the efficient CO release of Neu-MOF/Fla in tubes/cells and its potential as an anti-inflammatory reagent.

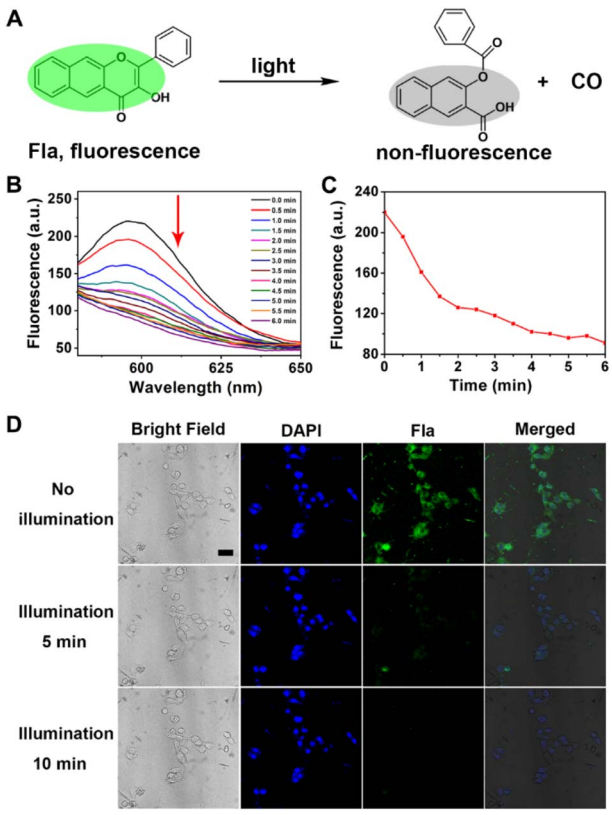

Fig. 3 (A) The schematic CO-releasing reaction of Fla. (B) Emission spectra of Neu-MOF/Fla (50 μg mL^{-1}) with light illumination for 6 min. (C) Linear curves of photo-induced emission changes in Neu-MOF/Fla (50 μg mL^{-1}). The emission wavelength being monitored was 596 nm. (D) Fluorescence images of BV2 cells exposed to Neu-MOF/Fla (50 μg mL^{-1}) with light illumination for different times. Scale bar = 25 μm.

As revealed in previous studies, MOF-808 has been an excellent heterogeneous catalyst for the catalytic hydrolysis of the peptide bond in many peptides.[49,63,64] In view of the critical role of Aβ in AD pathogenesis, we then studied the ability of our MOF-808 as a nanozyme to hydrolyze $A\beta_{40}$ monomers *in vitro* (Fig. 4A). The matrix-assisted laser desorption/ionization time-of-flight mass spectrometry (MALDI-TOF MS) assay showed that the normalized peak intensity of $A\beta_{40}$ monomers at *m*/*z*: 4331.5 was significantly reduced after incubation with MOF-808 at 37 °C for 24 h (Fig. 4B). Moreover, several low molecular weight peaks were obviously observed, indicating the effective occurrence of $A\beta_{40}$ degradation when incubated with MOF-808 (Fig. 4C). The turbidity analysis exhibited similar results (Fig. S15†). In addition, the XRD patterns of MOF-808 after hydrolysis further indicated the stability of the MOF-808 hydrolytic nanozyme under our experimental conditions (Fig. S16†). The SEM images of MOF-808 after hydrolysis further showed that the morphology was retained, suggesting that the MOF-808 nanozyme had excellent stability over the hydrolytic process (Fig. S17†). These results may provide new opportunities for cytotoxic Aβ clearance and avoidance of plaque deposition in AD.

Having demonstrated the targeted CO release and effective Aβ degradation of Neu-MOF/Fla, we further investigated the ability of Neu-MOF/Fla to modulate microglia-associated neuroinflammation and dysfunction. Reactive gliosis and neuroinflammation are widely considered to be some of the key hallmarks of AD, as resident immune cells in the brain, microglia, play an important role in brain function and

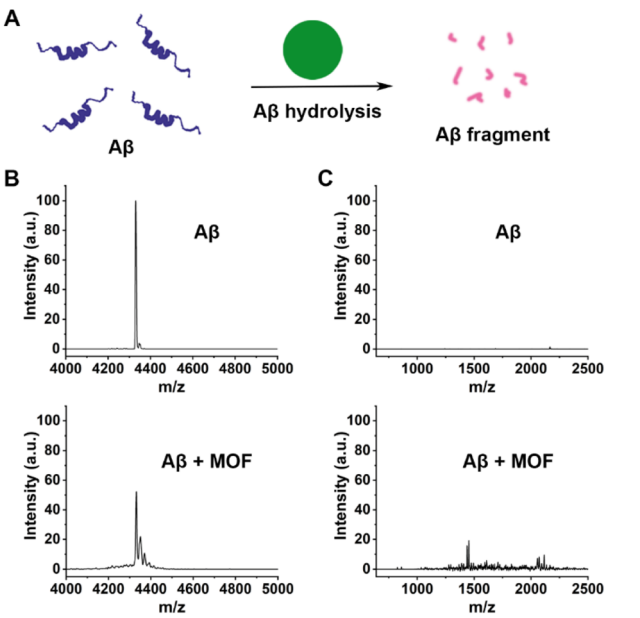

Fig. 4 (A) Schematic representation of the Aβ hydrolysis catalyzed by MOF nanozymes. (B and C) MALDI-TOF-MS analysis of the $A\beta_{40}$ monomers incubated with/without the MOF nanozymes for 24 h.

dysfunction.[65,66] It is estimated that the changes in the microglia cell phenotype affect the progression of the disease to some extent. In a healthy brain, the anti-inflammatory phenotype (responsible for expressing anti-inflammatory cytokines, degrading toxic proteins, such as amyloid plaques, and continually surveying the local environment) is activated trying to maintain brain homeostasis. However, during the course of neurodegeneration, there is a switch to the pro-inflammatory phenotype, upregulating the level of inflammatory cytokines, resulting in aggravation of the disease process.[67–69] Thus, we investigated the cell phenotype and the pro-inflammatory cytokine levels of BV2 cells with or without treatment of Neu-MOF/Fla in Aβ-induced inflammation. The anti-CD16 antibody (PE) was used to evaluate the pro-inflammatory phenotype while the anti-CD206 antibody (FITC) was used to evaluate the anti-inflammatory phenotype of BV2 cells. As shown in Fig. 5A and B, no obvious CD16 or CD206 signal was observed in BV2 cells treated under normal conditions (control); however, the BV2 cells treated with Aβ displayed a distinct CD16 signal, indicating that most BV2 cells switched from a homeostatic status to the pro-inflammatory phenotype. Notably, treatment with Neu-MOF/Fla and light illumination significantly enhanced CD206 signaling, and the signal of CD16 was totally quenched. Meanwhile, the immunofluorescence intensity ratio between CD206 and CD16 changed from 0.37 to 2.54 (Fig. 5C). Additionally, the bright field images showed that the cell morphology was reversed after treatment with Neu-MOF/Fla and light illumination (Fig. 5A), which was closely related to phagocytic function of microglia. These studies suggested that Neu-MOF/Fla regulated the pro-inflammatory to anti-inflammatory microglia polarization in the Aβ-induced inflammatory process. In addition, we further evaluated the expression of typical pro-inflammatory cytokines, TNF-α and IL-1β, up-regulated in BV2 cells activated with Aβ, which decreased significantly upon treatment with Neu-MOF/Fla and light illumination (Fig. 5D). This may be attributed to the targeted CO release and effective Aβ degradation of Neu-MOF/Fla. Overall, the results suggested that Neu-MOF/Fla was able to beneficially modulate pro-inflammatory microglial phenotypes and suppress neuroinflammation for pleiotropic neuroprotection.

The efficacy of Neu-MOF/Fla in ameliorating pathological characteristics of AD was further evaluated using a 3xTg-AD mouse model. Prior to *in vivo* evaluation, Cy5-labelled Neu-MOF/Fla was used to investigate the BBB permeability. The images of the brain and major organs showed that Neu-MOF/Fla successfully crossed the BBB and accumulated in brain parenchyma (Fig. S18†). We next conducted Morris water maze (MWM) experiments to evaluate the ability of Neu-MOF/Fla to restore cognitive function in 3xTg-AD mice. Here, a two-photon approach was employed to trigger CO release from administered Neu-MOF/Fla because of the low phototoxicity and deep tissue penetration.[60] Compared with AD mice, mice treated with Neu-MOF/Fla and light illumination exhibited shortened escape latency, increased crossing number and time at the target quadrant, and spatially oriented swimming behavior (Fig. 6A–D). Moreover, immunofluorescence staining of Aβ showed that the Aβ plaques was diminished in the brains of

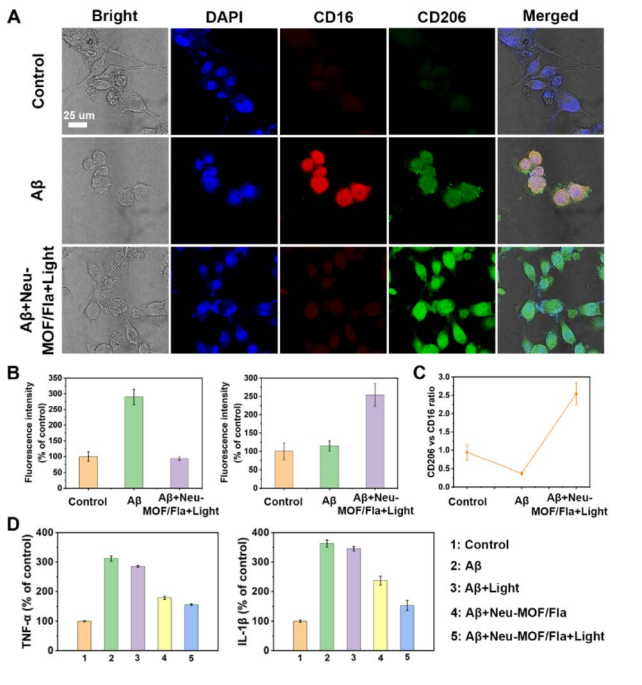

Fig. 5 (A) Confocal images of BV2 cells immunostained by pro-inflammatory phenotype biomarker CD16 and anti-inflammatory phenotype biomarker CD206 with different treatments. (B) Corresponding fluorescence intensity. (C) CD206 to CD16 immunity ratio with different treatments. (D) Anti-inflammatory effects of Neu-MOF/Fla in BV2 cells with different treatments.

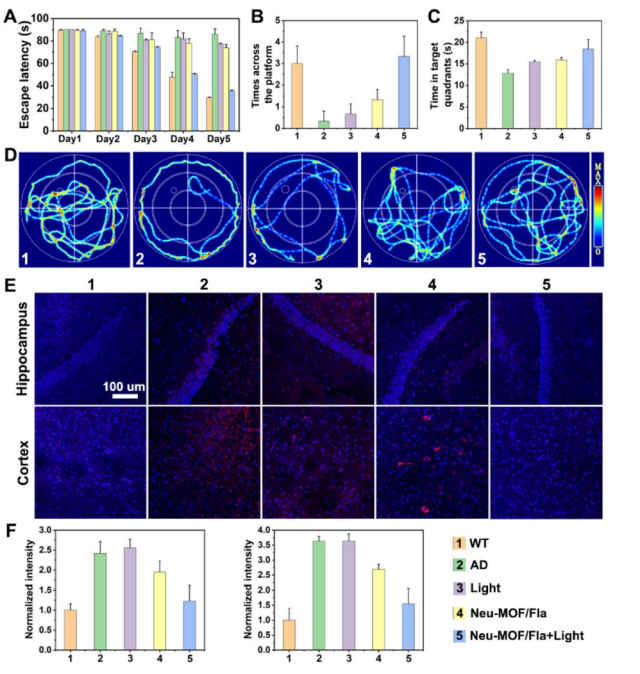

Fig. 6 (A) Escape latency. (B) The number of times the mice crossed the platform. (C) Time spent in the target quadrant. (D) Representative swimming paths of mice in the probe test. (E) Immunofluorescence of Aβ in the hippocampus and cortex of 3xTg-AD mice with different treatments. (F) Corresponding normalized fluorescence intensity.

3xTg-AD mice treated with Neu-MOF/Fla and light illumination compared to that of other groups (AD, Light, Neu-MOF/Fla) (Fig. 6E). Furthermore, the increased immunofluorescence of CD206 in the "Neu-MOF/Fla + Light" group revealed that Neu-MOF/Fla alleviated the neuroinflammation and reduced the reactive gliosis in the brain of 3xTg-AD mice (Fig. S19†). In addition, no evident potential toxicity was observed under our experimental conditions, suggesting the good biocompatibility of our system *in vivo* (Fig. S20–S22†). Overall, these investigations with 3xTg-AD mice models demonstrated that the biocompatible Neu-MOF/Fla significantly improved cognitive defects, mitigated the Aβ burden, beneficially modulated pro-inflammatory microglial phenotypes and suppressed the neuroinflammation.

Conclusions

In summary, we have constructed Neu-MOF/Fla and demonstrated its therapeutic potential for AD treatment. Unlike the reported nanoparticles that have limited accumulation in the brain based on the modified targeting ligands (such as antibodies, peptides or small molecules), Neu-MOF/Fla can recognize the pathological inflammatory signals of AD, and deliver the photo-triggered anti-inflammatory CO and MOF based hydrolytic nanozymes to the lesion area of the brain in a spontaneous manner. The photo-trigger released CO significantly inhibits neuroinflammation. Meanwhile, the MOF based hydrolytic nanozyme is responsible for clearance of Aβ. As a result, Neu-MOF/Fla strongly suppresses neuroinflammation, mitigates the Aβ burden, beneficially modulates pro-inflammatory microglial phenotypes and improves cognitive defects in 3xTg-AD mice. Moreover, blood biochemistry and histology analysis indicate Neu-MOF/Fla has no obvious toxicity under our experimental conditions. Therefore, our work provides new insights on the design of biomimetic multifunctional nanotherapeutics for the treatment of AD by means of amelioration of multiple symptoms and improvement of cognitive defects.

Data availability

The data that support the findings of this study are available from the corresponding author upon reasonable request.

Author contributions

X. Q. and J. R. conceived the project. C. L. carried out the experiments, analyzed the data and drafted the manuscript. W. Z., H. Z., C. Z. and X. D. helped collect some of the experimental data. All authors have given approval to the final version of the manuscript. C. L. and W. Z. contributed equally to this work.

Conflicts of interest

The authors declare no competing financial interests.

Acknowledgements

Financial support was provided by the National Key R&D Program of China (2019YFA0709202 and 2021YFF1200700), the National Natural Science Foundation of China (21820102009, 22237006, and 22122704), and the Jilin Innovation Project (2023DJ02).

References

1 R. N. Kalaria, G. E. Maestre, R. Arizaga, R. P. Friedland, D. Galasko, K. Hall, J. A. Luchsinger, A. Ogunniyi, E. K. Perry, F. Potocnik, M. Prince, R. Stewart, A. Wimo, Z. X. Zhang, P. Antuono and World Federation of Neurology Dementia Research, *Lancet Neurol.*, 2008, **7**(9), 812–826.
2 K. S. Kosik, T. J. Sejnowski, M. E. Raichle, A. Ciechanover and D. Baltimore, *Science*, 2016, **353**(6302), 872–873.
3 J. Gaugler, B. James, T. Johnson, J. Reimer, M. Solis, J. Weuve, R. F. Buckley and T. J. Hohman, *Alzheimer's Dementia*, 2022, **18**(4), 700–789.
4 J. A. Hardy and G. A. Higgins, *Science*, 1992, **256**(5054), 184–185.
5 D. J. Selkoe and J. Hardy, *EMBO Mol. Med.*, 2016, **8**(6), 595–608.
6 T. Arai, T. Araya, D. Sasaki, A. Taniguchi, T. Sato, Y. Sohma and M. Kanai, *Angew. Chem., Int. Ed.*, 2014, **53**(31), 8236–8239.
7 S. S. Jiao, X. Q. Yao, Y. H. Liu, Q. H. Wang, F. Zeng, J. J. Lu, J. Liu, C. Zhu, L. L. Shen, C. H. Liu, Y. R. Wang, G. H. Zeng, A. Parikh, J. Chen, C. R. Liang, Y. Xiang, X. L. Bu, J. Deng, J. Li, J. Xu, Y. Q. Zeng, X. Xu, H. W. Xu, J. H. Zhong, H. D. Zhou, X. F. Zhou and Y. J. Wang, *Proc. Natl. Acad. Sci. U.S.A.*, 2015, **112**(16), 5225–5230.
8 Y. Kwon, J. Shin, K. Nam, J. S. An, S. H. Yang, S. H. Hong, M. Bae, K. Moon, Y. Cho, J. Woo, K. Park, K. Kim, J. Shin, B. Y. Kim, Y. Kim and D. C. Oh, *Angew. Chem., Int. Ed.*, 2020, **59**(51), 22994–22998.
9 D. J. Hayne, S. Lim and P. S. Donnelly, *Chem. Soc. Rev.*, 2014, **43**(19), 6701–6715.
10 V. Armiento, A. Spanopoulou and A. Kapurniotu, *Angew. Chem., Int. Ed.*, 2020, **59**(9), 3372–3384.
11 J. Sevigny, P. Chiao, T. Bussiere, P. H. Weinreb, L. Williams, M. Maier, R. Dunstan, S. Salloway, T. Chen, Y. Ling, J. O'Gorman, F. Qian, M. Arastu, M. Li, S. Chollate, M. S. Brennan, O. Quintero-Monzon, R. H. Scannevin, H. M. Arnold, T. Engber, K. Rhodes, J. Ferrero, Y. Hang, A. Mikulskis, J. Grimm, C. Hock, R. M. Nitsch and A. Sandrock, *Nature*, 2016, **537**(7618), 50–56.
12 M. Zhang, X. Mao, Y. Yu, C. X. Wang, Y. L. Yang and C. Wang, *Adv. Mater.*, 2013, **25**(28), 3780–3801.
13 P. C. Ke, E. H. Pilkington, Y. Sun, I. Javed, A. Kakinen, G. Peng, F. Ding and T. P. Davis, *Adv. Mater.*, 2020, **32**(18), e1901690.
14 F. Panza, M. Lozupone, G. Logroscino and B. P. Imbimbo, *Nat. Rev. Neurol.*, 2019, **15**(2), 73–88.

15 D. Jeremic, L. Jimenez-Diaz and J. D. Navarro-Lopez, *Ageing Res. Rev.*, 2021, **72**, 101496.
16 G. M. McKhann, D. S. Knopman, H. Chertkow, B. T. Hyman, C. R. Jack Jr, C. H. Kawas, W. E. Klunk, W. J. Koroshetz, J. J. Manly, R. Mayeux, R. C. Mohs, J. C. Morris, M. N. Rossor, P. Scheltens, M. C. Carrillo, B. Thies, S. Weintraub and C. H. Phelps, *Alzheimers Dement*, 2011, **7**(3), 263–269.
17 Y. Huang and L. Mucke, *Cell*, 2012, **148**(6), 1204–1222.
18 V. Calsolaro and P. Edison, *Alzheimers Dement.*, 2016, **12**(6), 719–732.
19 R. M. Ransohoff, *Nature*, 2017, **552**(7685), 342–343.
20 J. Flores, A. Noël, B. Foveau, J. Lynham, C. Lecrux and A. C. LeBlanc, *Nat. Commun.*, 2018, **9**(1), 3916.
21 E. Check, *Nature*, 2002, **415**(6871), 462.
22 J. Cummings, G. Lee, A. Ritter, M. Sabbagh and K. Zhong, *Alzheimers Dement.*, 2020, **6**(1), e12050.
23 H. Akiyama, S. Barger, S. Barnum, B. Bradt, J. Bauer, G. M. Cole, N. R. Cooper, P. Eikelenboom, M. Emmerling, B. L. Fiebich, C. E. Finch, S. Frautschy, W. S. Griffin, H. Hampel, M. Hull, G. Landreth, L. Lue, R. Mrak, I. R. Mackenzie, P. L. McGeer, M. K. O'Banion, J. Pachter, G. Pasinetti, C. Plata-Salaman, J. Rogers, R. Rydel, Y. Shen, W. Streit, R. Strohmeyer, I. Tooyoma, F. L. Van Muiswinkel, R. Veerhuis, D. Walker, S. Webster, B. Wegrzyniak, G. Wenk and T. Wyss-Coray, *Neurobiol. Aging*, 2000, **21**(3), 383–421.
24 M. T. Heneka, M. J. Carson, J. E. Khoury, G. E. Landreth, F. Brosseron, D. L. Feinstein, A. H. Jacobs, T. Wyss-Coray, J. Vitorica, R. M. Ransohoff, K. Herrup, S. A. Frautschy, B. Finsen, G. C. Brown, A. Verkhratsky, K. Yamanaka, J. Koistinaho, E. Latz, A. Halle, G. C. Petzold, T. Town, D. Morgan, M. L. Shinohara, V. H. Perry, C. Holmes, N. G. Bazan, D. J. Brooks, S. Hunot, B. Joseph, N. Deigendesch, O. Garaschuk, E. Boddeke, C. A. Dinarello, J. C. Breitner, G. M. Cole, D. T. Golenbock and M. P. Kummer, *Lancet Neurol.*, 2015, **14**(4), 388–405.
25 L. A. Welikovitch, S. Do Carmo, Z. Magloczky, J. C. Malcolm, J. Loke, W. L. Klein, T. Freund and A. C. Cuello, *Proc. Natl. Acad. Sci. U.S.A.*, 2020, **117**(12), 6844–6854.
26 J. Y. Hur, G. R. Frost, X. Wu, C. Crump, S. J. Pan, E. Wong, M. Barros, T. Li, P. Nie, Y. Zhai, J. C. Wang, J. Tcw, L. Guo, A. McKenzie, C. Ming, X. Zhou, M. Wang, Y. Sagi, A. E. Renton, B. T. Esposito, Y. Kim, K. R. Sadleir, I. Trinh, R. A. Rissman, R. Vassar, B. Zhang, D. S. Johnson, E. Masliah, P. Greengard, A. Goate and Y. M. Li, *Nature*, 2020, **586**(7831), 735–740.
27 S. K. Baker, Z. L. Chen, E. H. Norris, A. S. Revenko, A. R. MacLeod and S. Strickland, *Proc. Natl. Acad. Sci. U.S.A.*, 2018, **115**(41), E9687–E9696.
28 L. E. Otterbein, F. H. Bach, J. Alam, M. Soares, H. T. Lu, M. Wysk, R. J. Davis, R. A. Flavell and A. M. K. Choi, *Nat. Med.*, 2000, **6**(4), 422–428.
29 X. Ji, C. Zhou, K. Ji, R. E. Aghoghovbia, Z. Pan, V. Chittavong, B. Ke and B. Wang, *Angew. Chem., Int. Ed.*, 2016, **55**(51), 15846–15851.
30 U. Shefa, D. Kim, M. S. Kim, N. Y. Jeong and J. Jung, *Neural Plast.*, 2018, **2018**, 1824713.
31 A. Nakao, D. J. Kaczorowski, B. S. Zuckerbraun, J. Lei, G. Faleo, K. Deguchi, K. R. McCurry, T. R. Billiar and S. Kanno, *Biochem. Biophys. Res. Commun.*, 2008, **367**(3), 674–679.
32 A. Fernandez-Fierro, S. C. Funes, M. Rios, C. Covian, J. Gonzalez and A. M. Kalergis, *Int. J. Mol. Sci.*, 2020, **22**(1), 294.
33 K. Fujita, M. Yamafuji, Y. Nakabeppu and M. Noda, *Oxid. Med. Cell. Longev.*, 2012, **2012**, 324256.
34 L. Li, J. Guo, Y. Wang, X. Xiong, H. Tao, J. Li, Y. Jia, H. Hu and J. Zhang, *Adv. Sci.*, 2018, **5**(10), 1800781.
35 U. Hasegawa, A. J. van der Vlies, E. Simeoni, C. Wandrey and J. A. Hubbell, *J. Am. Chem. Soc.*, 2010, **132**(51), 18273–18280.
36 Q. He, D. O. Kiesewetter, Y. Qu, X. Fu, J. Fan, P. Huang, Y. Liu, G. Zhu, Y. Liu, Z. Qian and X. Chen, *Adv. Mater.*, 2015, **27**(42), 6741–6746.
37 C. Yao, W. Wang, P. Wang, M. Zhao, X. Li and F. Zhang, *Adv. Mater.*, 2018, **30**(7), 1704833.
38 G. Yang, L. Xu, Y. Chao, J. Xu, X. Sun, Y. Wu, R. Peng and Z. Liu, *Nat. Commun.*, 2017, **8**(1), 902.
39 G. Wu, J. Zhang, Q. Zhao, W. Zhuang, J. Ding, C. Zhang, H. Gao, D. W. Pang, K. Pu and H. Y. Xie, *Angew. Chem., Int. Ed.*, 2020, **59**(10), 4068–4074.
40 M. Liang, K. Fan, M. Zhou, D. Duan, J. Zheng, D. Yang, J. Feng and X. Yan, *Proc. Natl. Acad. Sci. U.S.A.*, 2014, **111**(41), 14900–14905.
41 H. Wei and E. Wang, *Chem. Soc. Rev.*, 2013, **42**(14), 6060–6093.
42 J. Wu, X. Wang, Q. Wang, Z. Lou, S. Li, Y. Zhu, L. Qin and H. Wei, *Chem. Soc. Rev.*, 2019, **48**(4), 1004–1076.
43 M. Ma, Z. Liu, N. Gao, Z. Pi, X. Du, J. Ren and X. Qu, *J. Am. Chem. Soc.*, 2020, **142**(52), 21702–21711.
44 H. Wu, L. Liu, L. Song, M. Ma, N. Gu and Y. Zhang, *ACS Nano*, 2019, **13**(12), 14013–14023.
45 M. Li, J. Chen, W. Wu, Y. Fang and S. Dong, *J. Am. Chem. Soc.*, 2020, **142**(36), 15569–15574.
46 L. Ma, F. Jiang, X. Fan, L. Wang, C. He, M. Zhou, S. Li, H. Luo, C. Cheng and L. Qiu, *Adv. Mater.*, 2020, **32**(49), e2003065.
47 L. Zhang, Z. Liu, Q. Deng, Y. Sang, K. Dong, J. Ren and X. Qu, *Angew. Chem., Int. Ed.*, 2021, **60**(7), 3469–3474.
48 S. Li, Z. Zhou, Z. Tie, B. Wang, M. Ye, L. Du, R. Cui, W. Liu, C. Wan, Q. Liu, S. Zhao, Q. Wang, Y. Zhang, S. Zhang, H. Zhang, Y. Du and H. Wei, *Nat. Commun.*, 2022, **13**(1), 827.
49 H. G. T. Ly, G. Fu, A. Kondinski, B. Bueken, D. De Vos and T. N. Parac-Vogt, *J. Am. Chem. Soc.*, 2018, **140**(20), 6325–6335.
50 Z. Liu, L. Zhang, T. Cui, M. Ma, J. Ren and X. Qu, *Angew. Chem., Int. Ed.*, 2021, **60**(28), 15436–15444.
51 Q. Zhang, D. Dehaini, Y. Zhang, J. Zhou, X. Chen, L. Zhang, R. H. Fang, W. Gao and L. Zhang, *Nat. Nanotechnol.*, 2018, **13**(12), 1182–1190.
52 J. Xue, Z. Zhao, L. Zhang, L. Xue, S. Shen, Y. Wen, Z. Wei, L. Wang, L. Kong, H. Sun, Q. Ping, R. Mo and C. Zhang, *Nat. Nanotechnol.*, 2017, **12**(7), 692–700.

53 B. Rossi, G. Constantin and E. Zenaro, *Immunobiology*, 2020, **225**(1), 151865.
54 G. C. Kretzschmar, V. Bumiller-Bini, M. A. Gasparetto Filho, Y. R. Zonta, K. S. T. Yu, R. L. R. de Souza, L. A. Dias-Melicio and A. B. W. Boldt, *Front. Mol. Biosci.*, 2021, **8**, 630869.
55 S. N. Anderson, J. M. Richards, H. J. Esquer, A. D. Benninghoff, A. M. Arif and L. M. Berreau, *ChemistryOpen*, 2015, **4**(5), 590–594.
56 L. S. Lazarus, H. J. Esquer, A. D. Benninghoff and L. M. Berreau, *J. Am. Chem. Soc.*, 2017, **139**(28), 9435–9438.
57 Z.-Q. Li, J.-C. Yang, K.-W. Sui and N. Yin, *Mater. Lett.*, 2015, **160**, 412–414.
58 C. Liu, Z. Du, M. Ma, Y. Sun, J. Ren and X. Qu, *iScience*, 2020, **23**(9), 101483.
59 J. Park, S. H. Baik, I. Mook-Jung, D. Irimia and H. Cho, *Front. Immunol.*, 2019, **10**, 2231.
60 Y. Li, Y. Shu, M. Liang, X. Xie, X. Jiao, X. Wang and B. Tang, *Angew. Chem., Int. Ed.*, 2018, **57**(38), 12415–12419.
61 M. S. Diamond and T. A. Springer, *J. Cell Biol.*, 1993, **120**(2), 545–556.
62 S. Orden, C. De Pablo, C. Rios-Navarro, M. A. Martinez-Cuesta, J. E. Peris, M. D. Barrachina, J. V. Esplugues and A. Alvarez, *Chemother*, 2014, **69**(4), 995–1004.
63 D. Conic, K. Pierloot, T. N. Parac-Vogt and J. N. Harvey, *Phys. Chem. Chem. Phys.*, 2020, **22**(43), 25136–25145.
64 S. Dai, C. Simms, I. Dovgaliuk, G. Patriarche, A. Tissot, T. N. Parac-Vogt and C. Serre, *Chem. Mater.*, 2021, **33**(17), 7057–7066.
65 M. W. Salter and B. Stevens, *Nat. Med.*, 2017, **23**(9), 1018–1027.
66 T. Inoue, S. Saito, M. Tanaka, H. Yamakage, T. Kusakabe, A. Shimatsu, M. Ihara and N. Satoh-Asahara, *Proc. Natl. Acad. Sci. U.S.A.*, 2019, **116**(20), 10031–10038.
67 F. Zeng, Y. Wu, X. Li, X. Ge, Q. Guo, X. Lou, Z. Cao, B. Hu, N. J. Long, Y. Mao and C. Li, *Angew. Chem., Int. Ed.*, 2018, **57**(20), 5808–5812.
68 R. Martin-Rapun, L. De Matteis, A. Ambrosone, S. Garcia-Embid, L. Gutierrez and J. M. de la Fuente, *Curr. Pharm. Des.*, 2017, **23**(13), 1927–1952.
69 M. H. Park, M. Lee, G. Nam, M. Kim, J. Kang, B. J. Choi, M. S. Jeong, K. H. Park, W. H. Han, E. Tak, M. S. Kim, J. Lee, Y. Lin, Y. H. Lee, I. S. Song, M. K. Choi, J. Y. Lee, H. K. Jin, J. S. Bae and M. H. Lim, *Proc. Natl. Acad. Sci. U.S.A.*, 2019, **116**(47), 23426–23436.